Jul 5th, 12:00 AM - Jul 8th, 12:00 AM

Modelling Velocity Profiles of Aerated Flows Down Grassed Spillways

H. Cui
The University of New South Wales, hanwen.cui@adfa.edu.au

S. Felder
The University of New South Wales

M. Kramer
The University of New South Wales

8th International Junior Researcher and Engineer Workshop on Hydraulic Structures
ISBN 978-0-578-37416-1
https://doi.org/10.26077/bec3-52cb
Galway, Ireland,
5th - 8th June 2021

Modelling velocity profiles of aerated flows down grassed spillways

H. Cui[1,2], S. Felder[2] and M. Kramer[1]
[1] School of Engineering and Information Technology (SEIT)
UNSW Canberra
Canberra ACT 2610, AUSTRALIA
[2] Water Research Laboratory, School of Civil and Environmental Engineering
UNSW Sydney
AUSTRALIA
E-mail: hanwen.cui@adfa.edu.au

Abstract: *The ecological and environmental benefits of grassed spillways present a green solution to the construction of low head conveyance structures. On a grassed spillway, the aggregate of the grass canopy and root structure may alter flow resistance, velocity distribution and other flow properties. While subcritical flows in vegetated open channels have been extensively researched, only little is known about flow properties in supercritical high-velocity flows, which are typically characterized by self-aeration. The current study explores the application of a velocity superposition to supercritical aerated flows on a spillway with artificial grass. Velocity measurements were conducted with a Pitot tube and a phase-detection conductivity probe, allowing for the extraction of shear velocities at the canopy top which revealed an additional free-stream velocity layer. A comparison of the mixing layer length scale with the shear length scale (of the mixing layer) demonstrated a good correlation. Overall, this study provided new insights into the flow resistance of supercritical flows on grassed spillways.*

Keywords: *artificial grass, eco-friendly structures, flow resistance, high-velocity air-water flows, water sensitive urban design.*

1. INTRODUCTION

Grass linings on spillways and waterways with mild to moderate slopes provide ecological and environmental benefits such as ground water replenishment, vegetation growth (Mossa et al., 2017) and water quality improvement (Van Hemert et al., 2013). These advantages have promoted the use of grassed spillways for embankment protection (Wilcock et al., 1999), as agricultural floodway or small-scale drainage floodway (Van Hemert et al., 2013). The grass canopies act as roughness elements and enhance flow resistance, while the grass root structure provides additional support to the soil ground (Chen et al, 2012). In the past, flow resistance of grassed spillways was often investigated from a soil mechanics perspective, where the aggregate of soil and grass patches undergoes constant erosion and scouring damage (Ralston and Brevard, 1988). From a hydraulics point of view, subcritical flow conditions have been extensively researched with experimental and analytical modelling in both submerged and emergent conditions (Nepf, 2012) for various density (Guillén-Ludeña et al., 2020), expanding research of canopy flows into broader aspects of river floodplains (Crosato and Saleh, 2011) and tidal and coastal environments (Tinoco et al., 2020). Flow properties of grassed spillways under high-velocity supercritical flow conditions have received less attention.

In supercritical flows, the Froude number exceeds unity and turbulent energy obtained by the flows generates strong eddy motions, deforming the coherent free-surface that is maintained by surface tension and gravity (Brocchini and Peregrine, 2001). As turbulent forces dominate over surface tension and gravity, entrained air pockets break up into smaller air bubbles, a process termed self-aeration. Self-aeration on smooth spillways and the role of entrapped and entrained air was systematically described in Wilhelms and Gulliver (2005). Valero and Bung (2018) described the importance of free-surface instabilities on self-aeration in smooth and stepped spillways. However, self-aeration in flows down grassed spillways was only considered recently (Scheres et al. 2020). On grass-lined waterways, the supercritical flows can lead to erosion of the soil structure and engineering design guidelines must account for this as well as flow aeration. To provide a more controlled environment, the current study deployed a dense cover of artificial grass, allowing a detailed investigation into mean velocity profiles and flow resistance of grassed spillways.

Nikora et al. (2013) developed a model to characterize velocity profiles of flat grassed waterways in subcritical flows, which uses a linear superposition of several conventional concepts. In the present

study, the application of the velocity superposition of Nikora et al. (2013) was applied to supercritical flows on a spillway with artificial grass. The results revealed an additional free-surface layer, which led to an expansion of Nikora's et al. (2013) subcritical flow model. In addition, shear velocities at the canopy top were extracted through log-law fitting, demonstrating a good agreement with shear velocities evaluated from the friction slope, providing new information on the local flow resistance.

2. METHODOLOGY

2.1. Velocity superposition

The current study investigated the superposition of streamwise velocity profiles in supercritical free-surface flows down grassed spillways. The velocities in the water phase were superposed using conventional concepts after Nikora et al. (2013), including (i) a uniform velocity distribution inside the canopy layer, (ii) the mixing layer region, (iii) the logarithmic layer and (iv) the wake function; the current study proposes an additional (v) free-surface layer to reflect the interfacial velocity of free-surface waves.

The velocity distribution within the canopy is governed by the vegetational drag (with drag coefficient $C_d = 1.0$), further depending on the frontal area of grass per unit volume ($a = 281$ 1/m) and the channel slope ($S_0 = 0.19$). Herein, the single-phase model of Nikora et al. (2013) was applied up to the characteristic flow depth Y_1 where the void fraction is first measured ($C(Y_1) \approx 0.01$):

$$\bar{u}_{UD} = \begin{cases} \left(\frac{gS_0}{0.5\, C_d\, a}\right)^{0.5} & \text{if } 0 < y < Y_1 \\ 0 & \text{else} \end{cases} \quad (1)$$

where $\bar{u}_{UD}$ is a quasi-constant velocity (Nikora et al.,2004; Nepf, 2012; Nikora et al., 2013) and y is the bed-normal coordinate. The mixing layer includes the appearance of an inflection point and the velocity distribution $\bar{u}_{ML}$ is governed by a Kelvin-Helmholtz instability, generating mixing layer eddies (Raupach et al., 1996; Nepf, 2012; Nikora et al., 2013):

$$\bar{u}_{ML} = \begin{cases} (\bar{u}_i - \bar{u}_{UD})\left(1 + \tanh\frac{y-y_i}{L_e}\right) & \text{if } 0 < y < Y_1 \\ 0 & \text{else} \end{cases} \quad (2)$$

where $\bar{u}_i$ stands for the velocity at the inflection point, y_i is the location of the inflection point and L_e is a characteristic length scale of the mixing layer. The logarithmic layer follows a classical logarithmic velocity profile $\bar{u}_{LL}$, expressed as (Nikora et al. (2013):

$$\bar{u}_{LL} = \begin{cases} u_{*c}\,\frac{1}{\kappa}\ln\frac{y-y_i-d_i}{y_0} & \text{if } y_i + y_0 + d_i < y < Y_1 \\ 0 & \text{else} \end{cases} \quad (3)$$

where u_{*c} represents the shear velocity at the top of the canopy as a momentum transport scale, κ is the von Karman constant ($\kappa = 0.41$), d_i is the distance between the log layer and the inflection point and y_0 is the hydraulic roughness height, respectively. The wake function $\bar{u}_{WF}$ can be approximated as (Monin and Yaglom, 1971):

$$\bar{u}_{WF} = \begin{cases} u_{*c}\,\frac{2\Pi}{\kappa}\sin^2\frac{\pi y}{2Y_1} & \text{if } y_i + y_0 + d_i < y < Y_1 \\ 0 & \text{else} \end{cases} \quad (4)$$

where $\bar{u}_{WF}$ is the velocity of the wake and Π is the Coles wake parameter (Coles, 1956). The combination of these components provides a semi-analytical description of the velocity profile on grassed channels, as defined by for subcritical flow conditions:

$$\bar{u} = \bar{u}_{UD} + \bar{u}_{ML} + \bar{u}_{LL} + \bar{u}_{WF} \quad (5)$$

Supercritical flows on chutes are characterized by high velocities and shallow flow depths. In these flows, turbulence is generated at the bed boundary and leads to free-surface roughness, deformation and breakup once turbulence overcomes the two stabilizing factors, i.e., gravity and surface tension (Brocchini and Peregrine, 2001). In the present experiments, an additional layer of constant velocity ($\bar{u}_{FS}$) was observed, which was superposed to Nikora's et al. (2013) velocity superposition model, describing the near-surface region of the water column where free-surface instabilities and waves were observed:

$$\bar{u}_{FS} = \begin{cases} \bar{u}_{UD} + (\bar{u}_i - \bar{u}_{UD})\left(1 + \tanh\frac{Y_1 - y_i}{L_e}\right) + \frac{u_{*c,LL}}{\kappa}\left(\ln\frac{Y_1 - y_i - d_i}{y_0} + 2\Pi\right) & \text{if } Y_1 < y < Y_{90} \\ \text{else } 0 \end{cases} \quad (6)$$

where Y_{90} is the characteristic bed-normal depth where $C = 0.90$. A conceptual drawing of the velocity superposition from the bed to the free-surface is shown in Figure 1, and the complete velocity profile is defined as:

$$\bar{u} = \bar{u}_{UD} + \bar{u}_{ML} + \bar{u}_{LL} + \bar{u}_{WF} + \bar{u}_{FS} \quad (7)$$

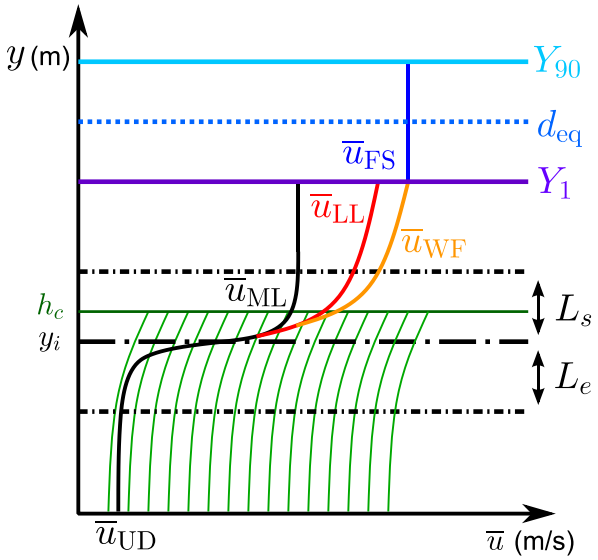

Figure 1 – Conceptual drawing of the velocity profile; additional parameters are the equivalent clear water depth (d_{eq}), the deflected grass height (h_c), the shear length scale of the mixing layer (L_s), and the mixing layer length scale (L_e)

2.2. Experimental facility and instrumentation

Experiments were performed in a laboratory chute at the UNSW Water Research Laboratory (WRL), which was 8 m long, 0.8 m wide and had a slope of 10.8 degrees. As shown in Figure 2a, the surface of the chute was equipped with a dense layer of artificial grass whose stems were uniformly attached to an underlying mesh. Herein, a specific flow rate of q = 0.188 m²/s was used, leading to a deflected grass height h_c = 20 mm. The flow rate was monitored with an ABB electromagnetic flow meter with uncertainty of ± 0.4%. The flow conditions corresponded to a Reynolds number $Re = q/\nu$ = 1.88 × 10⁵,a Froude number $Fr = \langle\bar{u}\rangle/(g\ d_{eq})^{1/2}$ 2.63 which was measured in the uniform flow region, i.e. at x = 7.5 m, with d_{eq} = 0.153 m being the equivalent clear water flow depth (Eq. 8). Note that parts of this dataset have been presented by Cui et al. (2020).

The flows just downstream of the weir crest were non-aerated and the free-surface was smooth, which was because surface tension was able to maintain the cohesion of the water phase (see Brocchini and Peregrine 2001). As the turbulence builds up, free-surface perturbations were observed at x = 2.1 m, leading to surface aeration at x = 3.8 m. In the non-aerated part of the spillway, the flow depth was

measured with a pointer gauge, while a dual-tip conductivity probe was used to estimate air concentration distributions (C) in regions with surface aeration, enabling the computation of d_{eq}:

$$d_{\mathrm{eq}} = \int_{y=0}^{y=Y_{90}} (1 - C)\,\mathrm{d}y \tag{8}$$

(a) (b)

Figure 2 – (a) Experimental chute with dense coverage of grass; (b) WRL dual-tip conductivity probe

The region above Y_{90} is commonly classified as the spray region, consisting of ejected water droplets that do not contribute significantly to the flow, and are therefore disregarded in the calculation of d_{eq} (Wood, 1983; Felder and Chanson, 2013). Water velocities were measured with a Pitot tube at 8 cross-sections, starting 0.5 m downstream of the weir crest with an interval of 1 m. In the air-water surface region, the Pitot tube data were complemented with interfacial velocities measured with a phase-detection conductivity probe. Herein, the same dual-tip conductivity probe as in Felder and Chanson (2018) was deployed, having a streamwise distance between the leading and trailing tip of Δx = 8.104 mm (Figure 2b), while the transverse distance was 1 mm. The probe was made in-house at the WRL and the inner and outer electrodes had diameters of 0.125 mm and 0.5 mm, respectively. Based upon a sensitivity analysis of sampling parameters, the phase-detection signals were recorded at a sampling frequency of 40 kHz for a duration of 180 s at each elevation. The signal processing for extracting velocities followed Kramer et al. (2019, 2020).

3. RESULTS

3.1. Velocity profiles

Figure 3 shows the development of streamwise velocity distributions along the grassed spillway for q = 0.188 m^2/s, comprising water velocities ($\bar{u}$) measured with the Pitot tube (hollow symbols) and interfacial velocities ($\bar{u}_{aw}$) measured with the dual-tip conductivity probe (solid symbols). The Pitot tube provided detailed velocity profiles in monophase flow regions, while the conductivity probe was able to measure the travel speed of surface deformations, waves and water droplets close to the free-surface, which had almost constant interfacial velocities (Figure 3). The velocity distributions evolved along the chute and approached uniform profiles towards the downstream end of the spillway. The equivalent clear water flow depth was calculated based upon the air-water flow data and the results are added in Figure 3, showing a small decline in d_{eq} towards the downstream end approaching uniform flow conditions. In the flow region where both instruments were able to measure velocities, the interfacial velocities agreed with the water velocities. Considering this close agreement, it can be assumed that $\bar{u}_{aw} \approx \bar{u}$.

The velocity profiles of three exemplary cross-sections at the end of the chute were compared against the model of Nikora et al. (2013) (Eq. 5) and the expanded model with the additional free-surface layer (Eq. 7) (Figure 4a). All velocities were normalized with the shear velocity at the channel bed u_* to highlight the universal agreement of the model with the velocity data. While the model of Nikora et al. (2013) fitted the experimental data well from the channel bed up to the wake region, the velocities

deviated in the free-surface region (Figure 4a). In contrast, the expanded model (Eq. 7) fitted the experimental data well across the full flow column.

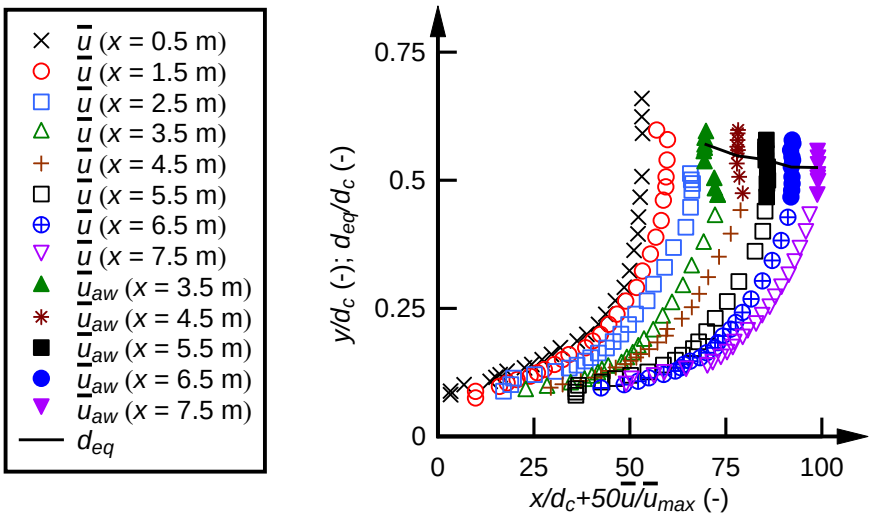

Figure 3 – Velocity profiles along the grassed spillway for q = 0.188 m²/s. Hollow symbols = Pitot tube data; solid symbols = dual-tip conductivity probe data

Figure 4b illustrates the corresponding dimensionless void fraction (C) and bubble count rate ($F/F_{\max}$) distributions, where $F_{\max}$ is the maximum bubble count rate in a cross section; both C and F were measured with the leading tip of the conductivity probe. Comparing the velocity data with the air-water flow properties shows that the presence of air-water interfaces in the form of entrapped air, free-surface roughness and waves in the upper part of the flows is represented by the constant interfacial velocity component (Eq. 6). The expanded model (Eq. 7) accounts for the air-water flow interactions and it is believed that this model is also applicable to grass-lined spillway flows with stronger aeration.

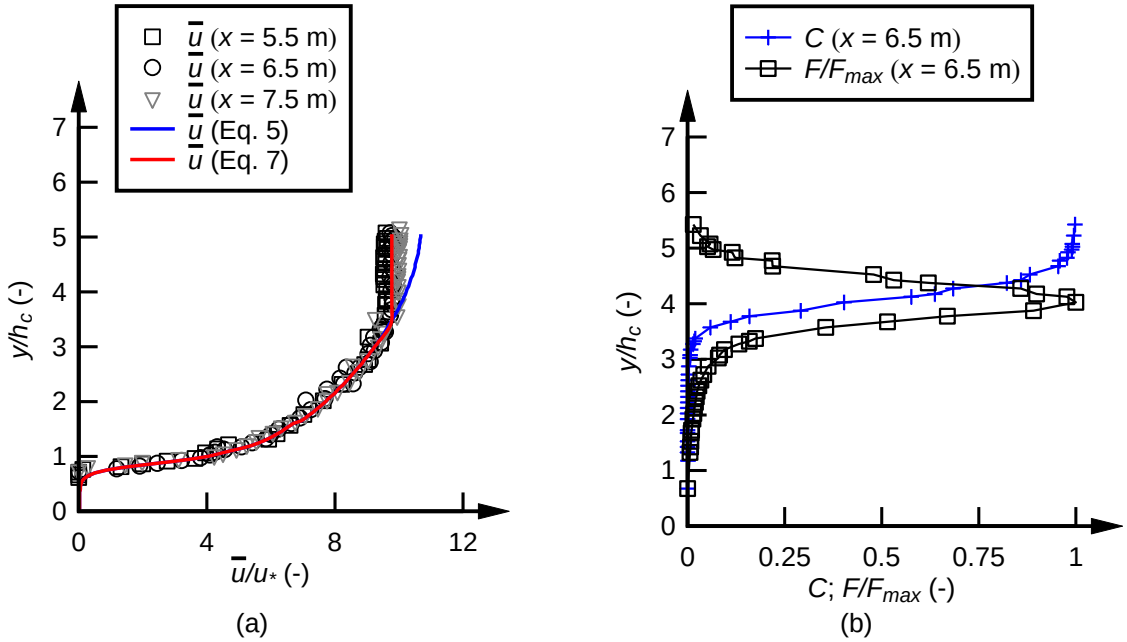

Figure 4 – (a) Comparison of supercritical velocity data at the downstream end with the model of Nikora et al. (2013) (Eq. 5) and the expanded model (Eq. 7) for q = 0.188 m²/st; (b) Corresponding void fraction (C) and bubble count rate (F) distributions.

3.2. Shear velocity

The shear velocity is commonly used to represent the bed shear stress of a flow, indicating the flow resistance. It has the same units as a velocity and is therefore often used for the normalization of velocity distributions (Figure 4a). The shear stress can be obtained by fitting the log law to the velocity profile which was conducted for the velocity distributions in the present study. The velocity profiles in the mixing and log layers agreed well with the model of Nikora et al. (2013) (Figure 4a). Using the dimensionless expression of u^+ and y^+, the measured velocities above $(y_i + d_i + y_0)$ and below the upper limit $((d - y_i - d_i) * 0.3 + y_i + d_i)$ were fitted to the log-law (Eq. 3), providing the shear velocities at the canopy top $u_{*,LL}$ (the subscript LL stands for log-law). The shear velocities at the canopy top ranged between 0.30 m/s $< u_{*c,LL} <$ 0.35 m/s, which was comparable to a micro-rough spillway with assorted grains (Severi, 2018).

Towards the downstream end of the spillway, the shear velocity from log law fitting ($u_{*c,LL}$) was compared with the shear velocity u_{*c}, derived from the channel slope assuming uniform flow conditions:

$$u_{*c} = \sqrt{\tau/\rho} = \sqrt{gS_0(d_{\text{eq}} - h_c)} \tag{10}$$

where τ is the shear stress at the canopy top and ρ is the density of water. Figure 5b shows this comparison, indicating good agreement between the two shear velocity estimates. Therefore, it appears that the log law fitting can be applied to grass-lined spillways. Future research must test if this is also valid for a wider range of flow conditions and for more strongly aerated flows on vegetated spillways.

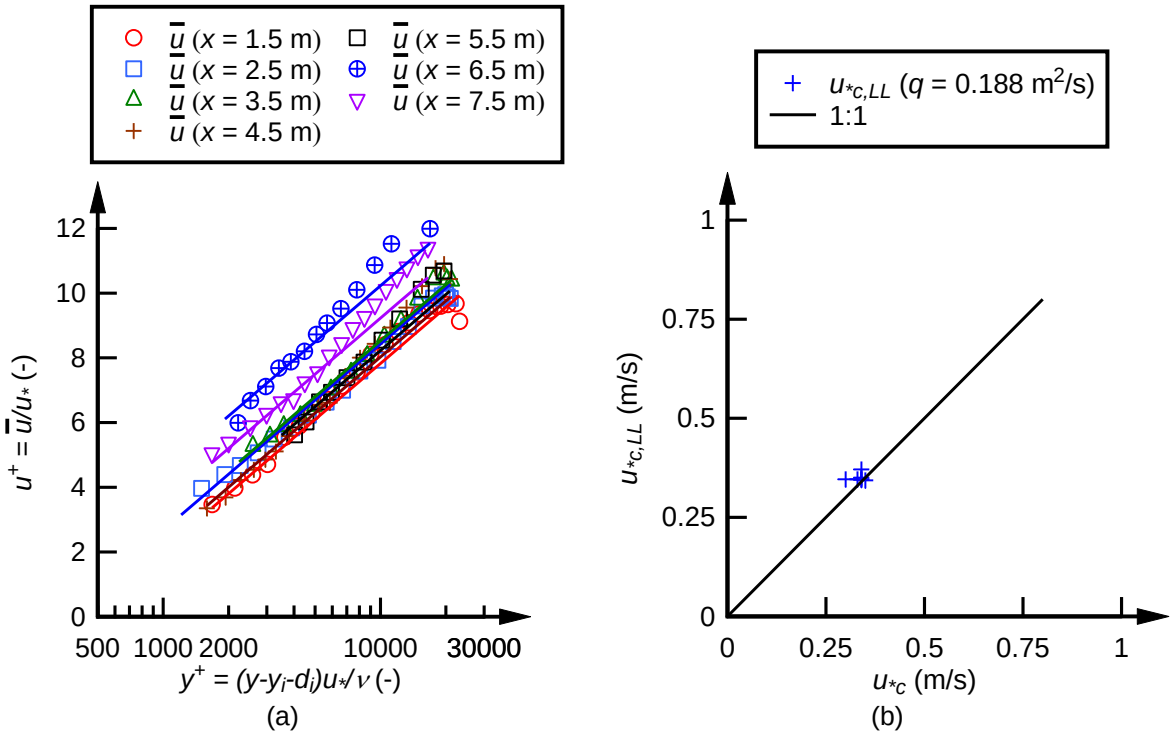

Figure 5 – (a) Comparison of the velocity data with the log law; (b) Comparison of shear velocities extracted from the log layer fitting $u_{*,LL}$ with shear velocities u_{*c} calculated with Eq. (10).

4. DISCUSSION: MIXING LAYER LENGTH SCALE

The mixing layer represents the coflowing zone of inside- and outside-canopy flows which generate vortex motions as Kelvin-Helmholtz waves (Raupach et al., 1996). It depicts an inflectional velocity profile featuring the transition between the uniform velocity profile (inside-canopy) to the log law velocity profile (outside-canopy). The mixing layer of a grassed channel was modeled with a hyperbolic function

(Eq. 2) by Nikora et al. (2013), where the mixing layer velocity becomes constant at $y > y_i + L_s$ (Figure 1). L_s is defined as the shear length scale of the mixing layer (Raupach et al., 1996; Nikora et al., 2013), indicating the region where the inflectional mixing layer applies (Figure 1). According to Raupach et al. (1996) and Nikora et al. (2013), the shear length scale of the mixing layer can be determined via:

$$L_s = \bar{u}_i / \left(\frac{\Delta \bar{u}}{\Delta y}\right)_{y_i} \quad (11)$$

Computed by a forward differences method, the shear length scale of the mixing layer L_s reflects the above-canopy section of the canopy-scale vortices (Figure 1). Whereas the mixing layer length scale L_e in Eq. (2) resembles the penetration of canopy-scale vortices into the grass canopy (Ghisalberti and Nepf, 2002). Under the assumptions that (i) the inflection point is in the middle of the mixing layer, and (ii) that the uniform velocity $\bar{u}_{UD}$ is much smaller than $\bar{u}_i$, both length scales should be identical, implying that the thickness of the mixing layer is $\delta_m = L_e + L_s = 2 * L_e = 2 * L_s$ (Raupach et al., 1996; Nikora et al. (2013)).

Herein, the velocities measured with the Pitot tube were used to calculate L_e and L_s applying Eqns. (2) and (11) respectively, and the calculated values are compared in Figure 6. Previous data of L_e and L_s of Nikora et al. (2013) for subcritical flows were added as well as the suggested relationship between L_e and L_s (Nikora et al., 2013) (Figure 6). The present length scales compared similarly to the observations of Nikora et al. (2013) (Figure 6). The close agreement between L_e and L_s confirms the statement from Raupach et al. (1996) and Nikora et al. (2013) that the shear length scale of mixing layer is also representative of the mixing layer thickness and the equivalency of L_e and L_s in the current configuration. The present supercritical flows were much shallower compared to subcritical flow conditions. Irrespective of this, the close agreement between sub- and supercritical flow observations of L_e and L_s extended the mixing layer concept to high-velocity flows on grassed spillways.

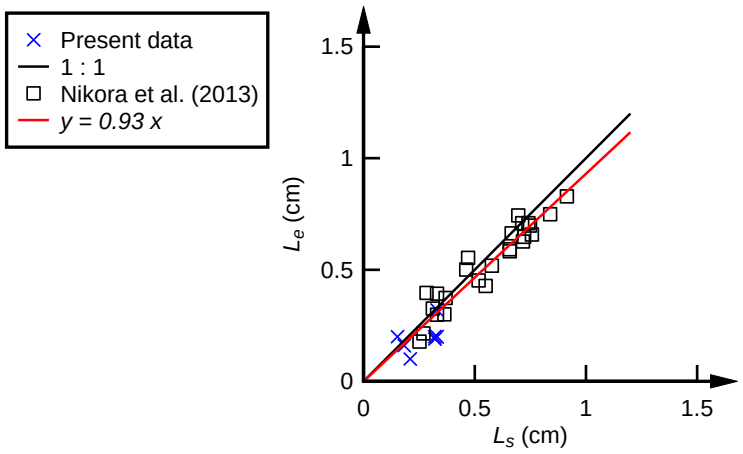

Figure 6 – Comparison of mixing layer length scales L_e (Eq. 2) and shear length scale of mixing layer L_s (Eq. 11) of the present study together with previous results from Nikora et al. (2013).

5. CONCLUSION

Detailed experiments of flows down a grass-lined spillway were conducted, providing new insights into the velocity distributions and shear velocities. The velocity profiles were obtained through measurements with a Pitot tube and a dual-tip conductivity probe, comprising a data set of both non-aerated flows close to the channel bed and aerated flows close to the free-surface. Both velocity measurement methods complemented each other and provided reliable velocity profiles across the full flow column. The present data were compared with the predicted velocity profile by Nikora et al. (2013). While the present data were well fitted from the bed to the wake layer, the model was expanded to the free-surface region characterized by free-surface roughness, entrained air and free-surface waves. Fitting the velocity profile to the log law provided the shear velocity estimate for grass-lined spillways, which was similar to spillway flows with a micro-rough bed. The mixing layer length scale was compared

with the shear length scale indicating close agreement of the two in supercritical flows. Overall, the present study provided novel insights into the flow resistance of grassed spillways through a detailed assessment of velocity distributions, which will be expanded to a wider range of flow conditions including real vegetation in future research.

6. ACKNOWLEDGMENTS

The authors would like to thank Rob Jenkins and Larry Paice (WRL, UNSW Sydney) for their technical assistance.

REFERENCES

Brocchini, M., Peregrine D.H. (2001). The dynamics of strong turbulence at free surfaces. Part 1. Description. Journal of Fluid Mechanics, 449, 225-254.

Chen, S.C., Kuo, Y.M., Yen, H.C. (2012). Effect of submerged flexible vegetation and solid structure bars on channel bed scour. International Journal of Sediment Research, 27, 323–336.

Crosato, A., Saleh, M.S. (2011). Numerical study on the effects of floodplain vegetation on river planform style. Earth Surface Processes and Landforms, 36, 711-720.

Cui, H., Kramer, M., Felder, S. (2020). Velocity profiles on a grass-lined spillway in supercritical flow, Proc. 1st IAHR YPN Congress 2020, Spain Water and IWHR, China.

Felder, S., Chanson, H. (2013). Aeration, flow instabilities, and residual energy on pooled stepped spillways of embankment dams. Journal of Irrigation and Drainage Engineering, 139, 880–887.

Felder, S., Chanson, H. (2018). Air–water flow patterns of hydraulic jumps on uniform beds macroroughness. Journal of Hydraulic Engineering, 144(3), 04017068.

Ghisalberti, M., Nepf, H. M. (2002). Mixing layers and coherent structures in vegetated aquatic flows. Journal of Geophysical Research, 107(C2).

Guillén-Ludeña, S., Lopez, D., Mignot, E., Riviere, N. (2020). Flow resistance for a varying density of obstacles on smooth and rough beds. Journal of Hydraulic Engineering, 146(2), 4019059.

Kramer, M., Valero, D., Chanson, H., Bung, D.B. (2019). Towards reliable turbulence estimations with phase-detection probes: an adaptive window cross-correlation technique. Experiments in Fluids, 60(2).

Kramer, M., Hohermuth, B., Valero, D., Felder, S. (2020). Best practices for velocity estimations in highly aerated flows with dual-tip phase-detection probes, International Journal of Multiphase Flow, 126, 103228.

Monin, A.S., Yaglom, A.M. (1975). Statistical Fluid Mechanics: Mechanics of Turbulence. Volume 1. MIT Press, Boston.

Mossa, M., Ben Meftah, M., De Serio, F., Nepf, H.M. (2017). How vegetation in flows modifies the turbulent mixing and spreading of jets. Nature Scientific Reports, 7, 1–14.

Nepf, H.M. (2012). Flow and transport in regions with aquatic vegetation. Annual Review of Fluid Mechanics 44, 123–142.

Nikora, V., Koll, K., McEwan, I., McLean, S., Dittrich, A. (2004). Velocity distribution in the roughness layer of rough-bed flows. Journal of Hydraulic Engineering, 130, 1036–1042.

Nikora, N., Nikora, V., O'Donoghue, T. (2013). Velocity profiles in vegetated open-channel flows: combined effects of multiple mechanisms. Journal of Hydraulic Engineering, 139(10), 1021–1032.

Ralston, D.C., Brevard, J.A. (1988). Design and performance of earth spillways, Proc. The ASCE Hydraulics Division, Special Conference, 871–876.

Raupach, M., Finnigan, J., Brunei, Y. (1996). Coherent eddies and turbulence in vegetation canopies: The mixing-layer analogy. Boundary-Layer Meteorology, 78, 351–382.

Severi, A. (2018). Aeration Performance and Flow Resistance in High-Velocity Flows over Moderately Sloped Spillways with micro-rough bed. Ph.D. Thesis, School of Civil and Environmental Engineering, UNSW Sydney, Australia.

Scheres, B., Schuettrumpf, H., Felder, S. (2020). Flow resistance and energy dissipation in supercritical air-water flows down vegetated chutes. Water Resources Research, 56, 1–18.

Tinoco, R.O., San Juan, J.E., Mullarney, J.C. (2020). Simplification bias: lessons from laboratory and field experiments on flow through aquatic vegetation. Earth Surface Processes and Landforms, 45, 121–143.

Valero, D., Bung, D.B. (2018). Reformulating self-aeration in hydraulic structures: turbulent growth of free surface perturbations leading to air entrainment. International Journal of Multiphase Flow, 100, 127–142.

Van Hemert, H., Igigabel, M., Pohl, R., Sharp, M., Simm, J., Tourment, R., Wallis, M. (2013). The International Levee Handbook. Ciria C731.

Wilcock, R.J., Champion, P.D., Nagels, J.W., Croker, G.F. (1999). The influence of aquatic macrophytes on the hydraulic and physico-chemical properties of a New Zealand lowland stream. Hydrobiologia, 416, 203–214.

Wilhelms, S.C., Gulliver, J.S. (2005). Bubbles and waves description of self-aerated spillway flow. Journal of Hydraulic Research, 43(5), 522–531.

Wood, I.R. (1983). Uniform region of self-aerated flow. Journal of Hydraulic Engineering, 109(3), 447-461.

Wood, I.R., Ackers, P., Loveless, J. (1983). General method for critical point on spillways. Journal of Hydraulic Engineering, 109, 308–312.